applied optics

# Revealing the radial modes in vortex beams

Bereneice Sephton,[1,2] Angela Dudley,[1,2] and Andrew Forbes[1,2,*]

[1]CSIR National Laser Centre, P.O. Box 395, Pretoria 0001, South Africa
[2]School of Physics, University of Witwatersrand, Private Bag 3, Wits 2050, South Africa
*Corresponding author: andrew.forbes@wits.ac.za

Received 6 June 2016; revised 16 August 2016; accepted 30 August 2016; posted 30 August 2016 (Doc. ID 267851); published 23 September 2016

**Light beams that carry orbital angular momentum are often approximated by modulating an initial beam, usually Gaussian, with an azimuthal phase variation to create a vortex beam. Such vortex beams are well defined azimuthally, but the radial profile is neglected in this generation approach. Here, we show that a consequence of this is that vortex beams carry very little energy in the desired zeroth radial order, as little as only a few percent of the incident power. We demonstrate this experimentally and illustrate how to overcome the problem by complex amplitude modulation of the incident field.** 

***OCIS codes:*** (080.0080) Geometric optics; (080.4865) Optical vortices; (230.0230) Optical devices; (230.3720) Liquid-crystal devices.

http://dx.doi.org/10.1364/AO.55.007830

## 1. INTRODUCTION

For beams of the form $E_0(r)e^{-il\phi}$, Allen *et. al.* associated the index, $l$, with the orbital angular momentum (OAM) carried by light, where $\phi$ is the azimuthal angle and $r$ the radial coordinate [1]. Beams with the azimuthal mode ($e^{-il\phi}$) that adhere to the paraxial approximation are consequently known to contain a well-defined OAM of $l\hbar$ per photon [1,2]. These azimuthal modes are also known as vortex beams in light of the associated helical twisting of the wave front along the propagation axis [1,3,4]. Vortex beams have since found many important applications (most of which are highlighted in Refs. [4] and [2]), such as optical tweezing [5], laser material surface processing [6,7], quantum entanglement [8,9], optical communication [10–12], image processing [13], and quantum metrology [14]. The subsequent creation of these beams is of great interest, and a surfeit of techniques have been developed for their creation, including spiral phase plates [15], holograms [16], spatial light modulators [17], spiral Fresnel lenses [18], cylindrical lenses [16,17], q-plates [19–21], and directly inside the source [22]. In the utilization of these vortex beams, the radial structure is often disregarded, as the fundamental radial mode ($p = 0$) is a ubiquitous choice in OAM experiments, with few exceptions seen in the implementation and characterization of optical fibers [23] and, recently, a quantum random walk [24].

Here, the effect of the missing radial component is investigated and shown to have a deleterious effect on the spatial power distribution of the desired OAM modes. Standard approaches to creating such beams are revealed to manifest unwanted radial modes that can contain the majority of the energy. Furthermore, we show how to rectify this problem through complex amplitude modulation.

## 2. VORTEX BEAMS

A vortex beam may be written as an azimuthal phase variation with a Gaussian envelope in the generation (waist) plane:

$$\psi^l(r,\phi) = G(r)e^{-il\phi}, \tag{1}$$

where $G(r) = e^{-(r/w_0)^2}$ is the Gaussian envelope, $r$ is the radial coordinate, $w_0$ the Gaussian beam waist, and $e^{-il\phi}$ the azimuthal phase variation with associated OAM of $l\hbar$ per photon [1,2], where $l$ is a non-zero integer. It has been noted that vortex beams may also be expressed as a special case of hypergeometric Gaussian modes [25].

This vortex field, however is not a solution to the free-space wave equation, and as such, vortex beams are not eigenmodes of free space, resulting in the excitation of supplementary fields [26] and spatial polarization variance with propagation [27].

OAM-carrying beam structures fulfilling the conditions of the free-space paraxial wave equation include Bessel [28,29] and Laguerre–Gaussian (LG) modes [1,4,26], with which these general vortex beams may subsequently be compared. Analyses could be generalized to either of the mode types, but this paper will focus on the LG modes whereby the amplitude at the beam waist is given by [30]

$$\mathrm{LG}_{p,l} = \sqrt{\frac{2p!}{\pi w_0^2(p+|l|)!}}\underbrace{\left(\frac{r\sqrt{2}}{w_0}\right)^{|l|}L_p^{|l|}\left(\frac{2r^2}{w_0^2}\right)}_{\text{amplitude term}}e^{-\left(\frac{r}{w_0}\right)^2}e^{-il\phi}. \tag{2}$$

Here, $L_p^{|l|}(x)$ is the Laguerre polynomial of orders $p$ and $l$, where the radial index, indicating the number of radial nodes, is $p \geq 0$.

It can be seen that for pure LG vortex modes ($p = 0$), there is an additional amplitude term, $(r\sqrt{2}/w_0)^{|l|}$, that ensures the invariance associated with the eigenmodes as they propagate. Similar terms with the same effect are also present in Bessel–Gaussian and other beams that are eigenmodes of free space. It is often unappreciated that it is this radial amplitude term, which is dependent on the azimuthal index ($|l|$) and not the azimuthal phase term itself ($|l|\phi$), that is responsible for the characteristic beam core intensity null associated with vortex beams. The observation of a null in vortex beams without this amplitude term is instead due to high spatial frequencies induced by the helicity of the phase together with their attenuation due to the finite apertures in the optical system [31].

It is well known that an optical field may be expressed as a linear combination of basis modes [32–34]:

$$U(r) = \sum\nolimits_j c_j \psi_j(r), \tag{3}$$

where $r = (x, y)$ is the spatial coordinate in the transverse plane, and $\psi_j(r)$ represents the basis mode. The complex correlation coefficient $c_j = \rho_j e^{i\Delta\varphi_j}$ weighs the contribution of each of the basis modes, where $\rho_j$ is the corresponding mode amplitude and $\Delta\varphi_j$ the intermodal phase difference between the $j$th mode and a selected reference mode. It thus follows that the vortex beam (of a particular azimuthal index, $l$) may easily be expressed in terms of LG modes of the same azimuthal index:

$$U^l(r, \phi) = \sum\nolimits_p c_p \mathrm{LG}_{p,l}(r). \tag{4}$$

Here, $|c_p|^2$ yields the power weighting of the vortex beam among the LG modes and can be expressed as [25]

$$c_p = \sqrt{\frac{(p + |l|)!}{p!}} \frac{\Gamma\left(p + \frac{|l|}{2}\right)\Gamma\left(\frac{|l|}{2} + 1\right)}{\Gamma\left(\frac{|l|}{2}\right)\Gamma(p + |l| + 1)}, \tag{5}$$

where $\Gamma(x)$ is the gamma function. It is clear that the vortex beam is the sum of many radial modes in the LG basis, i.e., the same azimuthal index as the vortex beam but with several radial indices. The implication is that the power in the desired $p = 0$ mode can be very small, approaching zero as the azimuthal index increases.

The ensuing evaluation of the modes indicates a significant spread of the power distribution to the outer spatial distributions, increasing concomitantly with the input OAM content. In other words, rings around the central beam appear due to additional radial indices when analyzed in terms of LG modes. This is illustrated in Fig. 1, where the power content of each mode, radial and azimuthal, in the LG basis is shown for a given input azimuthal mode.

For example, an input vortex mode of $l = 1$ has only 78% of its energy in the $\mathrm{LG}_{0,1}$ mode, with the rest spread across higher radial modes. It can be seen from Fig. 1 that there is a clear increase in the modal spreading as the input OAM of the vortex beam is increased: an input vortex mode of $l = 10$ has only 0.4% of its energy in the $\mathrm{LG}_{0,10}$ mode. Consequently, a direct result of the missing amplitude term is an increase in the power distribution as the OAM content of the vortex beam increases. This is seen by the increased spread of blue over the $p$-values at higher OAM values. Observation of the low intensity also indicates a low power content in any one of the radial modes with a higher OAM. Furthermore, there is a movement of power concentration to higher radial modes with OAM, as evidenced by the lower intensity (black) for $p = [0, 2]$ of $l = [7, 10]$. In fact, beyond $l = 4$, the power content of the zeroth radial mode, the desired mode, is close to zero.

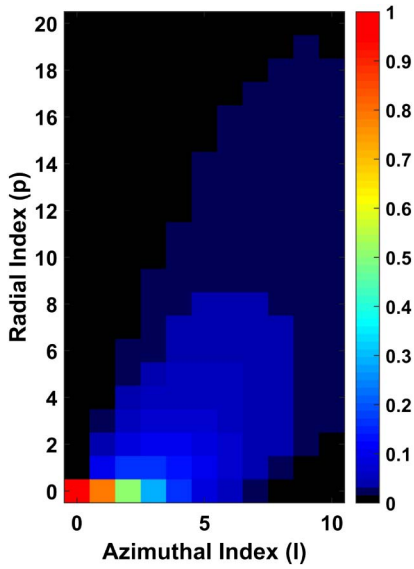


**Fig. 1.** Theoretical density plot, determined from Eq. (5), illustrating the spread of power into radial modes for vortex beams generated through phase-only transformations and thus lacking the amplitude term highlighted in Eq. (2).

## 3. EXPERIMENTAL METHODOLOGY AND RESULTS

### A. Methodology

Figure 2 displays the experimental setup for the generation and analysis of a vortex beam in terms of LG radial modes. Two steps were required for the experiment: generation of the vortex beams, and the subsequent decomposition into LG radial modes with the same azimuthal index.

#### 1. Beam Generation

To generate vortex beams, a horizontally polarized He–Ne laser of wavelength ~633 nm was expanded through a 10× objective lens and collimated by $L_1$ ($f_1 = 400$ mm) before being directed onto a reflective PLUTO-VIS HoloEye spatial light modulator (8 μm, 1920 × 1080 pixels, calibrated at a $2\pi$ phase shift for ~633 nm) marked as $SLM_1$. $SLM_1$ was programmed with an azimuthally varying phase profile, resulting in the first diffraction order possessing the required structure as given by Eq. (1). The addition of the quarter-wave plate (QWP) and q-plate (QP) seen in Fig. 2 allowed for the creation of vector vortex beams, which will be discussed later.

#### 2. Modal Decomposition

An important technique, essential for analyzing the generated beams in terms of LG modes, is modal decomposition. This

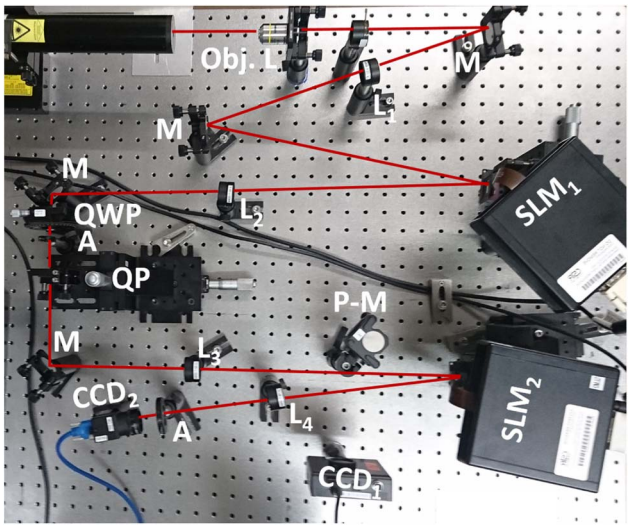


**Fig. 2.** Image of the experimental setup used to decompose the vortex beams into LG basis modes and measure the power distribution between radial modes. Obj. Lens, objective lens (10×); M, mirror; P-M, pop-up mirror; L, lens; SLM, spatial light modulator; A, aperture; QWP, quarter-wave plate; QP, q-plate ($q = 0.5$); CCD, camera.

technique is often used for characterizing beams, whereby any optical field may be expressed as a linear combination of basis modes, as described in Eq. (3). Here, we let the basis set be the chosen LG modes [Eq. (2)], allowing an arbitrary input field, $U(r)$, to be described by a weighted superposition of these modes. The orthonormality of the LG elements can be exploited to ascertain the weighting coefficients ($c_{p,l}$) by taking an inner product between the input field and desired LG mode [33,34]:

$$c_{p,l} = \langle U(r)|\mathrm{LG}_{p,l}(r)\rangle = \iint_{\mathbb{R}^2} U(r)\mathrm{LG}_{p,l}(r)^* \mathrm{d}^2 r, \quad (6)$$

where integration is over all space, and $\mathrm{LG}_{p,l}(r)^*$ is the complex conjugate of Eq. (2). The complex conjugate of a basis mode is often referred to as a match filter [35,36]. Determination of the coefficient in terms of the field reflected off of $\mathrm{SLM}_1$ ($U(r)\mathrm{LG}_{p,l}(r)^*$) is possible by taking the Fourier transform of Eq. (6) to yield

$$U_{p,l}(k_x, k_y) = \iint U(x,y)\mathrm{LG}_{p,l}(x,y)^* e^{-i(k_x x + k_y y)} \mathrm{d}x\mathrm{d}y, \quad (7)$$

where $k_x, k_y$ are wave vectors. The on-axis intensity at the Fourier plane (i.e., at the plane of $\mathrm{CCD}_2$) provides a physical measurement of the inner product given in Eq. (6). The on-axis point, $(k_x, k_y) = (0, 0)$, produces an expression equivalent to Eq. (6):

$$U_{p,l}(0,0) = \iint_{\mathbb{R}^2} U(r)\mathrm{LG}_{p,l}(r)^* \mathrm{d}^2 r = c_{p,l}. \quad (8)$$

It follows that the intensity at the field center, $I(0, 0)$, will then yield the power weighting (i.e., square of the weighting coefficient):

$$I_j^p(0,0) = |U_{p,l}(0,0)|^2 = |c_{p,l}|^2. \quad (9)$$

The characterization of the vortex beam only extends to the intensity correlations and not the intermodal phase decomposition. Therefore, for the scope of this paper, decomposition was restricted to determining only the amplitude terms, as described above.

Experimentally, the amplitude decomposition was obtained through the optical inner product measurement given in Eq. (6) between the experimental field, $U(r)$, generated by $\mathrm{SLM}_1$ and the match filter, $\mathrm{LG}_{p,l}(r) *$ on $\mathrm{SLM}_2$ with a thin lens performing the Fourier transformation. First, isolation and imaging of the first diffraction order onto the match filter ($\mathrm{SLM}_2$) was achieved through a $4f$ imaging system (lenses $\mathrm{L}_2$ ($f_2 = 300$ mm) and $\mathrm{L}_3$ ($f_3 = 300$ mm), with an aperture placed in the Fourier plane. The Fourier transform of the resultant field after $\mathrm{SLM}_2$ ($U(r)\mathrm{LG}_{p,l}(r)^*$) was achieved with lens $\mathrm{L}_4$ ($f_4 = 200$ mm). An aperture placed before $\mathrm{CCD}_2$ (PointGrey) isolated the first diffraction order, allowing the optical inner product to be recorded, where an on-axis signal dictated a correlation between the generated mode and match filter, while an on-axis null indicated a mismatch. A pop-up mirror (P-M), placed equidistant between $\mathrm{SLM}_2$ and $\mathrm{CCD}_1$ (Spiricon, LBA-FW-SCOR-7350115), was used to image the generated near field to facilitate the alignment of the optical elements.

### B. System Verification

Testing of the system alignment and subsequent confirmation of the associated technique was achieved by performing a modal decomposition on the $\mathrm{LG}_{p,0}$ and $\mathrm{LG}_{0,l}$ beams, where $p = [0, 7]$ and $l = [-4, 4]$. The intensities were detected at the origin of the Fourier plane by $\mathrm{CCD}_2$ positioned in this plane, after the Fourier transformation was carried out by $\mathrm{L}_4$. The intensity detected by a single pixel at the origin yielded the power measurement. It follows that direct correlation is expected whereby maximal intensity is detected at the origin of the Fourier plane for conjugate modes generated by $\mathrm{SLM}_1$ and $\mathrm{SLM}_2$, while null intensity is detected at the origin for all other modal combinations.

Figure 3 displays the system test results in the form of density plots. Here, the main red diagonals illustrate strong detection of the corresponding modes as expected, with negligible detected intensities for the non-correlating LG modes.

Crosstalk evidenced by off-axis intensities greater than 0 (light blue) seen in Fig. 3 is due to system misalignment and aberrations in the optical elements. This, however, is

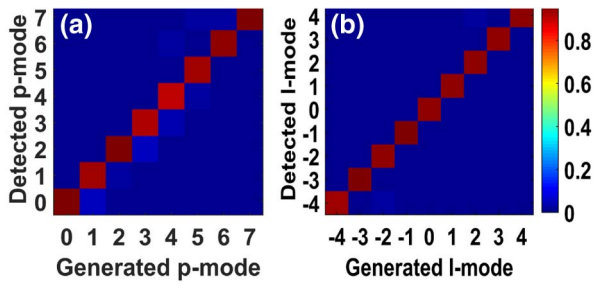


**Fig. 3.** Modal decomposition density plots for decomposition of radial (a) and OAM (b) LG modes of $p = [0, 7]$ and $l = [-4, 4]$, respectively, into the LG basis for determination of experimental system accuracy and reliability. The false colors indicate the fractional detected power, with the summation of intensities in each row yielding unity.

minimal, indicating good system alignment as well as minimal adverse aberrational effects. Consequently, a good degree of accuracy and reliability can be expected for modes detected by the system.

### C. Vortex Radial Fields

An $l = 1$ vortex structure (without the amplitude term) was generated by encoding $SLM_1$, as described earlier. Decomposition of the beam was performed for radial modes $p = [0, 7]$, which yielded values for the power coefficients described by Eq. (5). Figure 4 displays these experimental values in terms of percentages together with the theoretical values (blue curve) calculated from Eq. (5) for comparison.

The majority of the power (78.5%) is still retained within the fundamental radial order, with maximal distribution of the remaining power between the immediate adjacent radial modes. Summation over the theoretical power coefficients indicates that 95% of the total power falls within the $p \leq 4$ radial range. The experimental values are in excellent agreement with the expected theoretical values, as seen by close positioning of the respective data points and the maximum deviation of ~2% occurring within the system error at $p = 0$.

Similarly, encoding $SLM_1$ with a vortex structure of $l = 10$ [Eq. (1)] generated a vortex mode of high OAM for radial decomposition and analysis. Decomposition of the field was performed for LG radial modes $p = [0, 18]$. A plot of results similar to that of Fig. 4 is presented in Fig. 5 with a theoretical (blue curve) and experimental comparison (red data points).

Good agreement between the theoretical and experimental values is again evident with all experimental values (red) falling within an acceptable range of theoretical predictions (blue), as indicated by the error bars.

A significant shift and redistribution of power can be seen across the radial modes in comparison to $l = 1$ (Fig. 4) as a result of the higher OAM content. The power maximum being centered at $p = [7, 8]$ and a drop of ~78.1% power in the fundamental mode (as only 0.4% remains in this mode for Fig. 5) clearly illustrates this. Additionally, the maximum power carried in a single radial mode decreased by ~76.3%, as seen in the power difference between $p = 0$ (Fig. 4) and $p = 7$ (Fig. 5), indicating that ~76.3% more of the power is distributed amongst other modes than for a mode with an OAM of an order of magnitude less. Furthermore, summation over the first 50 theoretical power coefficients only yields 64% of the total beam power, and 95% can be seen to be spread over the first 500 radial modes.

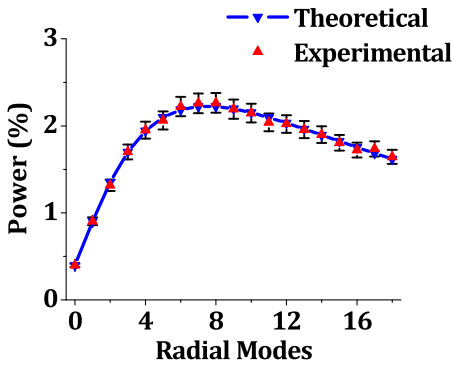


**Fig. 5.** Experimental and theoretical comparison of power weighting across radial modes = [0, 18] for a vortex mode of $l = 10$. The blue line (theoretical) is included to guide the eye.

Further experimentation, including the addition of a QWP and QP as depicted in Fig. 2, allowed for a special case of vector vortex modes to be tested. Such q-plates are now routinely used in laboratories to create scalar and vector vortex beams by imparting an azimuthal-only phase to the input beam, as was done with the SLM, but by geometric phase control [21] rather than dynamic phase control. We find identical results for the q-plate as reported here for the SLM. This is illustrated in Fig. 6, where the detected radial modes were removed for an $l = 1$ beam generated by the QP by passing a beam with the amplitude term pre-encoded such that the azimuthal term supplied by the QP creates an eigenmode of free space. It follows that 100% power is expected in the fundamental mode.

It can be seen that maximal intensity exists in the fundamental radial mode, confirming that it is the phase variation itself (the vortex) and not the manner in which it is implemented that matters. Aberrations present in the QP are detected as an additional radial mode ($p = 2$), causing the slight mismatch. It may thus be concluded that minimal aberrations were present in the QP and, as such, poor beam quality would be due to the unmodulated azimuthal-induced phase and not the quality of the QP itself.

Clear dissipation of the vortex beam power over an increasing number of radial modes can subsequently be seen with

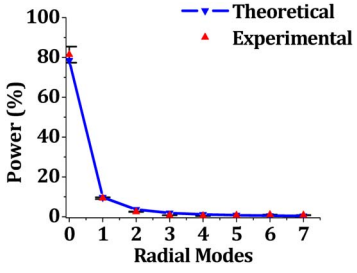


**Fig. 4.** Experimental and theoretical comparison of power weighting across radial modes $p = [0, 7]$ for a vortex mode of $l = 1$. The blue line (theoretical) is included to guide the eye. Error bars for $p > 0$ are too small to be observed.

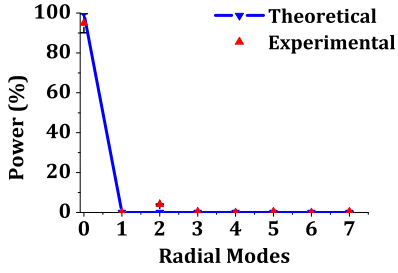


**Fig. 6.** Experimental and theoretical comparison of power weighting across radial modes $p = [0, 7]$ for a QP-generated vortex mode of $l = 1$ with the radial modes removed. The blue line (theoretical) is included to guide the eye. Error bars for $p > 0$ are too small to be observed.

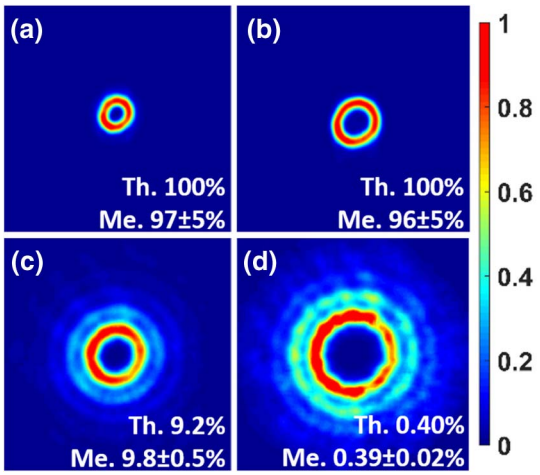


**Fig. 7.** Experimental far-field images of vortex beams (a) $l = 5$, (b) $l = 10$ containing the amplitude term and (c) $l = 5$, (d) $l = 10$ without the amplitude term, illustrating its effect on the retention of beam power within the lower order radial modes as well as encoded beam structure. Measured (Me.) and theoretical (Th.) values for the percentage power occurring in the $p = 0$ mode of the beam are displayed in the bottom-right corner. Intensities are normalized to the highest value for the individual images and thus are not indications of relative power differences between the beams.

beams of higher OAM content, which should inspire caution in their utilization and generation for high OAM experiments.

Images of the beams with (LG) and without (azimuthal-only vortex) the amplitude term of different OAM values ($l = 5$, 10) were taken in the far field for visual illustration of the amplitude term effect. This is presented in Fig. 7. The values shown on the bottom-right corners give the corresponding theoretical and experimental percentage powers contained in the desired $p = 0$ mode.

Figures 7(a) and 7(b) display $LG_{0,5}$ and $LG_{0,10}$ beams in the far field, where the power is seen to be confined to the fundamental radial mode, as expected. Comparison with the respective beams with missing amplitude terms [Figs. 7(c) and 7(d)] clearly show further radial power distribution by the supplementary rings. An increase in the shift of power to farther rings with an increase in OAM is also evident. Additionally, modes (c) and (d) are larger than the modes containing the amplitude term, demonstrating the distribution of maximal power to further radial modes, as the diameter of the radial mode with the peak power is then larger than the fundamental mode.

This is supported by the power values given in the bottom corners, where a very high percentage of the beam power is seen to be contained in the fundamental radial modes for beams (a) and (b), which contain the amplitude term, and much poorer percentages for beams (c) and (d), without the term. Furthermore, the percentage power in the $p = 0$ mode may be appraised as beam purity, where the amplitude-containing beams can be seen to have a high beam purity as opposed to the deteriorating purity apparent in the beams without this vital term.

Reconsidering the LG equation [Eq. (2)], it follows that one could expect the Laguerre term to be solely responsible for the radial power distribution, as it controls the radial degree of freedom ($p$). In the case where $p = 0$, however, this polynomial term reduces to 1 and subsequently has no effect on the radial distribution. Examining the OAM-modulated amplitude term, it could also be naively expected that it does not contribute to radial distribution, but upon comparing Eqs. (1) and (2), it is clear that for $p = 0$, this is the only non-constant term missing and thus is responsible for the difference observed between these azimuthal-only vortex beams and the LG beams, which are eigenmodes of free space. It follows that exclusion of this term removes the OAM-dependent amplitude modulation and forces nature to correct for it by introducing radial distributed fields that may be interpreted as additional radial modes in the LG basis. The spreading out of the beam power is subsequently a direct consequence of forcing nature to exact OAM modulation of the amplitude, whereby this unintended effect is rapidly enhanced with increased OAM content in the vortex beam.

Implications of this phenomenon can be deleterious for experimental work where beam power and mode purity are concerns, particularly when beams of higher OAMs are required. Generation of these missing-amplitude beams in such experiments could result in many issues, such as detection thresholds and increased measurement uncertainties as well as the number of optical components it will be possible to use in the experimental design. Due to this drastic power loss with OAM, utilization of these beams could additionally cause the beam power to become an issue in experiments where it would ordinarily not be a consideration.

In establishing amplitude modulation to prevent this, however, there will be initial overall transmissive and/or diffractive power losses induced by the methods currently available, including spatial light modulators, where there is a perceptible loss in beam power. Subsequently, consideration of experimental parameters is an important factor. Beams that are not of a small OAM result in radial power distributions to such a degree that the nature-inspired power loss far outweighs the loss induced by the technique required for introducing OAM amplitude modulation.

## 4. CONCLUSION

In conclusion, we have analyzed the radial distribution of azimuthal-only vortex beams through decomposition into radial LG basis modes and compared them to the mathematical structure of these eigenmodes. The results demonstrated a rapid increase in radial power divergence with OAM content along with a shift in the power maximum to farther radial positions. Corresponding deterioration of the mode purity was subsequently inferred. Further inspection between the modes led to the deduction that this phenomenon was the natural response to the absence of amplitude modulation by OAM. Subsequently, the presence of this amplitude term correlates to a counter-intuitive control of the radial power distribution. Awareness of this dissipation of beam power from the zeroth order is important for many experiments that require high levels of beam power in these radial modes as well as the solution to this problem by amplitude modulation.

## REFERENCES


1. L. Allen, M. W. Beijersbergen, R. J. C. Speeruw, and J. P. Woerdman, "OAM transformation Laguerre-Gaussian laser modes," Am. Phys. Soc. **45**, 8185–8188 (1992).
2. A. M. Yao and M. J. Padgett, "Orbital angular momentum: origins, behavior and applications," Adv. Opt. Photon. **3**, 161–204 (2011).
3. E. J. Galvez, B. L. Rojec, and K. R. McCullough, "Imaging optical singularities: Understanding the duality of C-points and optical vortices," Proc. SPIE **8637**, 863706 (2013).
4. M. W. Beijersbergen, L. Allen, H. E. L. O. van der Veen, and J. P. Woerdman, "Astigmatic laser mode converters and transfer of orbital angular momentum," Opt. Commun. **96**, 123–132 (1993).
5. H. He, M. E. J. Friese, N. R. Heckenberg, and H. Rubinsztein-Dunlop, "Direct observation of transfer of angular momentum to absorptive particles from a laser beam with a phase singularity," Phys. Rev. Lett. **75**, 826–829 (1995).
6. J. J. J. Nivas, S. He, A. Rubano, A. Vecchione, D. Paparo, L. Marrucci, R. Bruzzese, and S. Amoruso, "Direct femtosecond laser surface structuring with optical vortex beams generated by a q-plate," Sci. Rep. **5**, 17929 (2015).
7. O. J. Allegre, W. Perrie, S. P. Edwardson, G. Dearden, and K. G. Watkins, "Laser microprocessing of steel with radially and azimuthally polarized femtosecond vortex pulses," J. Opt. **14**, 085601 (2012).
8. A. Mair, A. Vaziri, G. Weihs, and A. Zeilinger, "Entanglement of the orbital angular momentum states of photons," Nature **412**, 313–316 (2001).
9. A. Vaziri, G. Weihs, and A. Zeilinger, "Superpositions of the orbital angular momentum for applications in quantum experiments," J. Opt. B **4**, S47–S51 (2002).
10. J. Wang, J.-Y. Yang, I. M. Fazal, N. Ahmed, Y. Yan, H. Huang, Y. Ren, Y. Yue, S. Dolinar, M. Tur, and A. E. Willner, "Terabit free-space data transmission employing orbital angular momentum multiplexing," Nat. Photonics **6**, 488–496 (2012).
11. B. Guan, R. P. Scott, C. Qin, N. K. Fontaine, T. Su, C. Ferrari, M. Cappuzzo, F. Klemens, B. Keller, M. Earnshaw, and S. J. B. Yoo, "Free-space coherent optical communication with orbital angular, momentum multiplexing/demultiplexing using a hybrid 3D photonic integrated circuit," Opt. Express **22**, 145–156 (2014).
12. G. Gibson, J. Courtial, M. Padgett, M. Vasnetsov, V. Pas'ko, S. Barnett, and S. Franke-Arnold, "Free-space information transfer using light beams carrying orbital angular momentum," Opt. Express **12**, 5448–5456 (2004).
13. J. A. Davis, D. E. McNamara, D. M. Cottrell, and J. Campos, "Image processing with the radial Hilbert transform: theory and experiments," Opt. Lett. **25**, 99–101 (2000).
14. V. D'Ambrosio, N. Spagnolo, L. Del Re, S. Slussarenko, Y. Li, L. C. Kwek, L. Marrucci, S. P. Walborn, L. Aolita, and F. Sciarrino, "Photonic polarization gears for ultra-sensitive angular measurements," Nat. Commun. **4**, 2432 (2013).
15. M. W. Beijersbergen, R. P. C. Coerwinkel, M. Kristensen, and J. P. Woerdman, "Helical-wave-front laser-beams produced with a spiral phaseplate," Opt. Commun. **112**, 321–327 (1994).
16. V. Y. Bazhenov, M. V. Vasnetsov, and M. S. Soskin, "Laser beams with screw dislocations in their wavefronts," JETP Lett. **52**, 429–431 (1990).
17. M. Reicherter, T. Haist, E. U. Wagemann, and H. J. Tiziani, "Optical particle trapping with computer-generated holograms written on a liquid-crystal display," Opt. Lett. **24**, 608–610 (1999).
18. M. Harris, C. A. Hill, P. R. Tapster, and J. M. Vaughan, "Laser modes with helical wave fronts," Phys. Rev. A **49**, 3119–3122 (1994).
19. B. Piccirillo, S. Slussarenko, L. Marrucci, and E. Santamato, "The orbital angular momentum of light: genesis and evolution of the concept and of the associated photonic technology," Riv. del Nuovo Cim. **36**, 501–555 (2013).
20. S. Slussarenko, A. Murauski, T. Du, V. Chigrinov, L. Marrucci, and E. Santamato, "Tunable liquid crystal q-plates with arbitrary topological charge," Opt. Express **19**, 4085–4090 (2011).
21. L. Marrucci, C. Manzo, and D. Paparo, "Optical spin-to-orbital angular momentum conversion in inhomogeneous anisotropic media," Phys. Rev. Lett. **96**, 163905 (2006).
22. D. Naidoo, F. Roux, A. Dudley, I. Litvin, B. Piccirillo, L. Marucci, and A. Forbes, "Controlled generation of higher-order Poincare sphere beams from a laser," Nat. Photonics **10**, 327–332 (2016).
23. O. Shapira, A. F. Abouraddy, J. D. Joannopoulos, and Y. Fink, "Complete modal decomposition for optical waveguides," Phys. Rev. Lett. **94**, 143902 (2005).
24. F. Cardano, F. Massa, E. Karimi, S. Slussarenko, D. Paparo, C. de Lisio, F. Sciarrino, E. Santamato, and L. Marrucci, "Photonic quantum walk in a single beam with twisted light," Sci. Adv. **1**, E150087 (2015).
25. E. Karimi, G. Zito, B. Piccirillo, L. Marrucci, and E. Santamato, "Hypergeometric-Gaussian modes," Opt. Lett. **32**, 3053–3055 (2007).
26. A. Forbes, *Laser Beam Propagation: Generation and Propagation of Customized Light* (CRC, 2014).
27. D. Yang and S. Wu, *Fundamentals of Liquid Crystal Devices* (Wiley, 2006).
28. J. Durnin, J. Miceli, and J. H. Eberly, "Diffraction-free beams," Phys. Rev. Lett. **58**, 1499–1501 (1987).
29. J. Arlt and K. Dholakia, "Generation of high-order Bessel beams by use of an axicon," Opt. Commun. **177**, 297–301 (2000).
30. B. E. Saleh and M. Teich, *Fundamentals of Photonics*, 2nd ed. (Wiley, 2007).
31. F. S. Roux, "Optical vortex density limitation," Opt. Commun. **223**, 31–37 (2003).
32. T. Kaiser, D. Flamm, S. Schröter, and M. Duparré, "Complete modal decomposition for optical fibers using CGH-based correlation filters," Opt. Express **17**, 9347–9356 (2009).
33. I. A. Litvin, A. Dudley, F. S. Roux, and A. Forbes, "Azimuthal decomposition with digital holograms," Opt. Express **20**, 10996–11004 (2012).
34. C. Schulze, S. Ngcobo, M. Duparré, and A. Forbes, "Modal decomposition without a priori scale information," Opt. Express **20**, 27866–27873 (2012).
35. D. Flamm, C. Schulze, D. Naidoo, S. Schroter, A. Forbes, and M. Duparre, "All-digital holographic tool for mode excitation and analysis in optical fibers," J. Lightwave. Technol. **31**, 1023–1032 (2013).
36. A. Forbes, A. Dudley, and M. McLaren, "Creation and detection of optical modes with spatial light modulators," Adv. Opt. Photon. **8**, 200–227 (2016).